Chapter 6 Analysis of Flow Direction Effects in a Single-Channel Serpentine Geometry for PEM Fuel Cells at the Cathode Side

Capítulo 6 Análisis de los efectos en la dirección del flujo en una geometría de serpentín de un canal para celdas de combustible tipo PEM en el lado del cátodo

CEBALLOS-PÉREZ, José[1], ORDÓÑEZ-LÓPEZ[1,*], Luis and SIERRA-GRAJEDA, Juan[2]

[1]Centro de Investigación Científica de Yucatán, Unidad de Energía Renovable, Parque Científico Tecnológico de Yucatán, Carretera Sierra Papacal – Chuburná Puerto, Km 5, Sierra Papacal, Mérida, Yucatán, México.
[2]Facultad de Ingeniería, Universidad Autónoma del Carmen, Campus III, Avenida Central S/N, Esq. con Fracc. Mundo Maya, C.P. 24115, Ciudad del Carmen, Campeche, México.

ID 1st Author: *José, Ceballos-Pérez* / **ORCID**: 0000-0001-7529-0346, **CVU CONAHCYT ID**: 928198

ID 1st Co-author: *Luis, Ordóñez-López* / **ORCID**: 0000-0003-1110-1934, **CVU CONAHCYT ID**: 43804

ID 2nd Co-author: *Juan, Sierra-Grajeda* / **ORCID**: 0000-0002-0565-6450, **CVU CONAHCYT ID**: 219284

DOI: 10.35429/H.2023.6.60.66

J. Ceballos, L. Ordóñez and J. Sierra

* lcol@cicy.mx

S. Vargas, S. Figueroa, C. Patiño and J. Sierra (AA. VV.) Engineering and Applied Sciences. Handbooks-TI-©ECORFAN-Mexico, Mexico City, 2023

Abstract

Proton Exchange Membrane (PEM) fuel cells represent a promising clean energy technology that converts hydrogen and oxygen into electricity with water as the sole byproduct. This work presents a comprehensive analysis of the impact of flow direction, specifically parallel flow and counter-flow configurations, on the performance of a single-channel serpentine geometry. The serpentine flow field pattern is widely utilized for its advantages in enhancing mass transport and reducing pressure drop. This study integrates computational fluid dynamics (CFD) simulations using an open-source toolbox based on C++ to investigate the influence of flow direction on the liquid water saturation distribution within the cell. The analysis of liquid water accumulation is essential, as it directly affects the overall performance and durability of the PEM fuel cell. Saturation contour maps are obtained at 0.52 V for each geometry. The results show that water saturation tends to accumulate at the edges of the electrode-membrane assembly, and the counter-parallel flow exhibits the major saturation distribution.

PEM fuel cell, OpenFOAM, CFD, Water saturation, Mass transport

Resumen

Las celdas de combustible de membrana de intercambio de protónico (PEM) representan una prometedora tecnología de energía limpia que convierte el hidrógeno y el oxígeno en electricidad con agua como único subproducto. Este trabajo presenta un análisis del impacto de la dirección del flujo, específicamente las configuraciones de flujo paralelo y contraflujo, en el rendimiento de una geometría de serpentín de un canal. La geometría tipo serpentín es ampliamente utilizada por sus ventajas para mejorar el transporte de masa y reducir la caída de presión. En este estudio, se integran simulaciones de dinámica de fluidos computacional (CFD) utilizando un código abierto basado en C ++ para investigar la influencia de la dirección del flujo en la distribución de saturación de agua líquida dentro de la celda. El análisis de la acumulación de agua líquida es esencial, ya que afecta directamente al rendimiento general y la durabilidad de la celda. Los mapas de contorno de saturación se obtienen a 0.52 V para cada geometría. Los resultados muestran que la saturación de agua tiende a acumularse en los bordes del conjunto electrodo-membrana, y el flujo contraparalelo exhibe la mayor distribución de saturación.

Celda tipo PEM, OpenFOAM, CFD, Saturación de agua, Transporte de masa

1. Introduction

Proton Exchange Membrane (PEM) fuel cells are a promising alternative as a clean energy technology, offering a pathway to sustainable power generation for various applications [1]. A PEM fuel cell is an electrochemical device that converts chemical energy directly into electrical energy through electrochemical reactions. The flow channels ensure optimal reactant distribution, efficient mass transport, and overall cell performance among these components. These flow channel designs consider flow directions and geometry, with flow and counter-flow configurations emerging as vital elements in serpentine channel designs[2]. Due to their simplicity and effectiveness, serpentine flow channels are of interest in PEM fuel cell design. In a serpentine flow channel, reactant gases traverse a winding path along the electrode surfaces, enhancing interaction between the gases and the catalyst layers. This geometry optimizes the utilization of catalyst sites while promoting efficient water management [3]. The reactant gases typically flow through these channels either in the same direction (co-flow) or opposite directions (counter-flow) to the serpentine path[4]. Understanding the implications of these flow configurations is crucial for maximizing fuel cell performance. In this work, three different fuel cell configurations are analyzed to observe the behavior of the polarization curves in a single-channel serpentine flow path with co-flow and counter-flow directions using OpenFOAM (Open Field Operation and Manipulation), an open-source toolbox based on C++, to solve a 3D multiphase non-isothermal model [5] with three different configurations of single-channel serpentine geometry and flow directions.

2. Methodology

A 3D representation of the computational domain of the numerical model is shown in Fig. 1. The domain consists of the main components of a PEM fuel cell: bipolar plates (BP), gas flow channels (GFC), gas diffusion layers (GDL), catalyst layers (CL), and the protonic membrane for both the anode and cathode; where the red line represents the location where the electrochemical reaction occurs.

Figure 1 Computational domain and its components

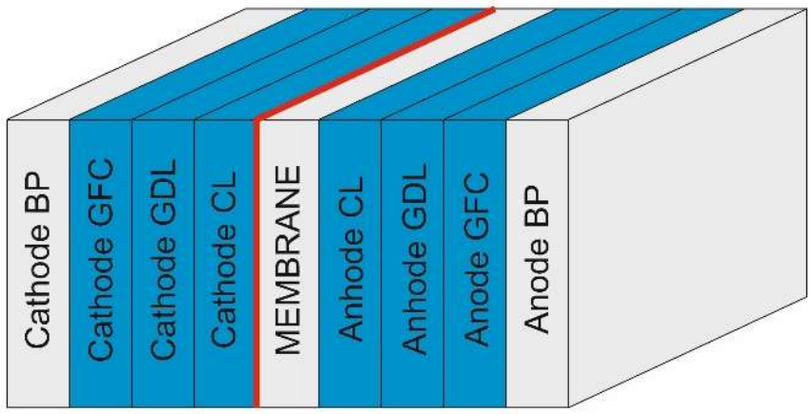

Table 1 shows the governing equations and source terms. Modeling the flow through the fuel cell components used the Navier-Stokes equations and considered isotropic porous media. For the continuity equation (Eq. 1), ρ_g is the fluid density, $\vec{U}_g$ the velocity vector, S_l is the mass source term due to phase change, where, in Eq. 2, C_r is the condensation rate, ε the porosity, s the water saturation, x_{WV} the water vapor mass fraction, p_{sat} water saturation pressure, R the ideal gas constant, M_{H_2O} stands for the molecular weight of water. In the momentum equation (Eq. 3) p_g, μ_g, and S_M represent the pressure gradient, dynamic viscosity, and momentum source term, respectively. S_M is the Darcy resistance in the porous media, where K_g is the permeability of the gas phase. In the species transport equation (Eq. 5) y_i and D_g^{eff} are the species i mass fraction and the effective diffusion coefficient of each gas, respectively. In the liquid water transport equation (Eq. 9), the terms D_l stands for the diffusivity of liquid water where ρ_l, k_l and μ_l represents the fluid density, thermal conductivity, and dynamic viscosity of liquid water, respectively, and p_c is the capillary pressure. For the energy equation (Eq. 6) $\rho_{mix}, C_{p_{mix}}, k_{mix}, T$, stands the fluid density of the gas mixture, the specific heat capacity of the gas mixture, the thermal conductivity of the gas mixture, and temperature, respectively. S_E^{reac} and S_E^{PC} are the energy source terms due to the heat released by the electrochemical reactions and water phase change, where δ_{MEA} is the membrane electrode assembly thickness, η_{act} are the activation losses, n is the number of electrons, F is the Faraday constant, and h_{mfg} is the latent heat.

Table 1 Governing equations

Description	Equation	
Continuity equation	$\nabla \cdot (\rho_g \vec{U}_g) = -S_l$	(1)
Mass source term due to phase change	$S_l = -C_r \frac{\varepsilon(1-s)(x_{WV} p_g - p_{sat})}{RT} M_{H_2O}$	(2)
Momentum equation	$\nabla \cdot (\rho_g \vec{U}_g \vec{U}_g) = -\nabla p_g + \nabla \cdot (\mu_g \nabla \vec{U}_g) + S_M$	(3)
Darcy source term	$S_M = -\frac{\mu_g \vec{U}_g}{K_g}$	(4)
Specie transport equation	$\nabla \cdot (\rho_g \vec{U}_g y_i) = (\nabla \cdot \rho_g D_g^{eff} \nabla y_i)$	(5)
Energy equation	$\nabla \cdot (\rho_{mix} C_{p_{mix}} \vec{U}_g T) = \nabla \cdot (k_{mix} \nabla T) + S_E^{reac} + S_E^{PC}$	(6)
Energy source term due to the heat released by the electrochemical reactions	$S_E^{reac} = \frac{1}{\delta_{MEA}} \left(\eta_{act} - \frac{T \nabla S}{nF} \right)$	(7)
Source term due to water phase change	$S_E^{PC} = S_l h_{mfg}$	(8)
Liquid water transport equation	$\nabla \cdot (\rho_l D_l \nabla s) - \nabla \cdot (\rho_g \vec{U}_g s) = S_l$	(9)
Diffusivity of liquid water	$D_l = \frac{\rho_l k_l}{\mu_l} \frac{\partial p_c}{\partial s}$	(10)

Table 2 summarizes the initial conditions for the steady-state simulation. Here, Dirichlet boundary conditions are applied at the fluid inlets for velocity, temperature, and mass fractions of both the anode and the cathode gas flow channels. Neumann boundary conditions are applied at the fluid outlets for mass fractions, temperature and saturation, with their gradients set to zero in the flow direction.

Table 2. Boundary and initial values

Component	Momentum	Energy	Species transport	Liquid water transport
Anode inlet	$U_{fuel} = 9\ \mathrm{m/s}$ $\nabla p_{air} = 0$	$T = 333\ K$	$y_{H_2} = 0.727$ $y_{H_2O} = 0.273$	$s = 0$
Anode outlet	$p_{air} = 506{,}625\ Pa$	$\nabla T = 0$	$\nabla y_{H_2} = 0$ $\nabla y_{H_2O} = 0$	$\nabla s = 0$
Cathode inlet	$U_{air} = 9\ \mathrm{m/s}$ $\nabla p_{air} = 0$	$T = 333\ K$	$y_{O_2} = 0.225$ $y_{H_2O} = 0.024$ $y_{N_2} = 0.751$	$s = 0$
Cathode outlet	$p_{air} = 506{,}625\ Pa$	$\nabla T = 0$	$\nabla y_{O_2} = 0$ $y\nabla_{H_2O} = 0$ $\nabla y_{N_2} = 0$	$\nabla s = 0$
Walls	$U = 0$	$T = 333\ K$	$\nabla y = 0$	$\nabla s = 0$

Figure 2 shows the different flow configurations to obtain the polarization curves with an open-source toolbox based on icoFoam, an OpenFOAM application that solves the incompressible laminar Navier-Stokes equations using the PISO algorithm and discretizes the equations based on the finite volume method. The Preconditioned bi-Conjugate Gradient (PBiCG) method was used to find convergence in the energy equation, and Preconditioned bi-Conjugate Gradient Stabilized (PBiCGStab) for other variables (continuity, momentum, species transport, energy, and liquid water transport). For all variables, the convergence criterion was a residual of $1x10^{-9}$.

Figure 2 Flow configurations for the different geometries of the single-channel serpentine flow paths

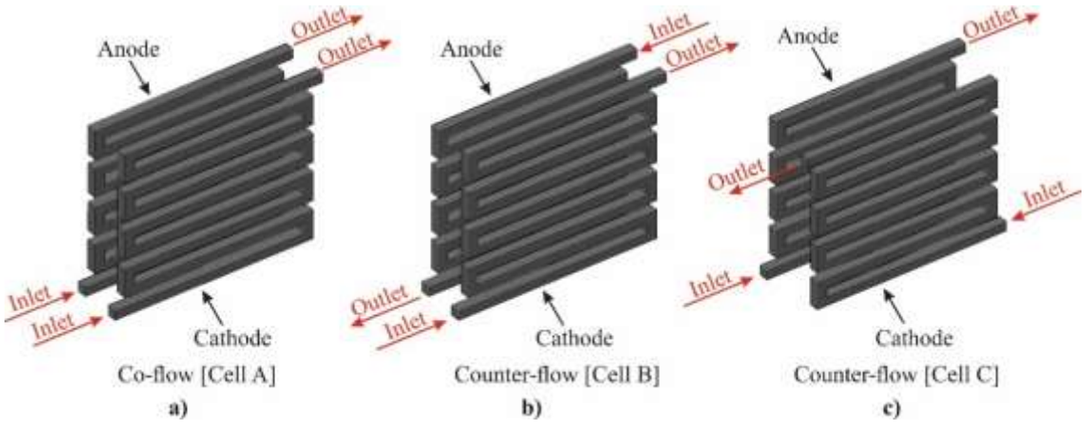

Results

Figure 3 shows the polarization curves where cell B exhibits the major current density, then cell A, and finally cell C. However, cell C performs a maximum current density at 0.52 V, where the calculation stops for this configuration. Therefore, the contour maps of the current density at the interface CL-membrane at the cathode side in Figure 4 are obtained at 0.52 V. It is noticed that even when cell B exhibits the greatest current density, the best distribution belongs to cell A. In other words, the best performance is shown by cell A, specifically in this study, where the difference between the current density of A and B is 0.53 %.

Figure 3 Polarization curves of the different flow configurations

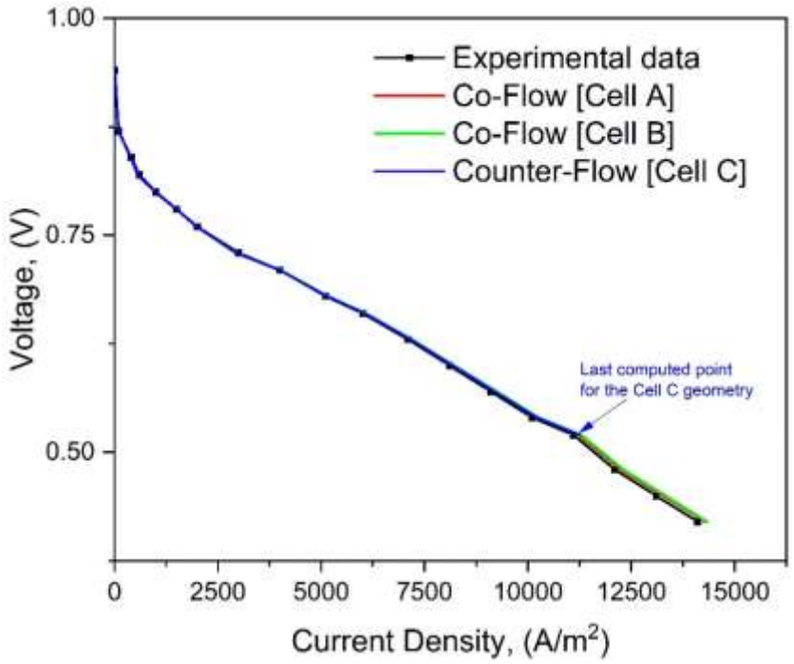

Figure 4 shows the distribution of the current density for the three flow configurations at 0.52 V, where it can be seen that cell B has a minor exploited active area. This is due to the delay of the reactant gases that need time to meet and associate the electrons and proton to form water at the cathode side. Therefore, cell A exhibits a better distribution with a parallel flow path between the anode and the cathode, even when the current density is lower. Cell C finds it challenging to reach the maximum point of the experimental data due to the limits of the model and the attempt to simulate complex geometries with the same work conditions.

Cell A's co-flow configuration offers a uniform distribution and guarantees a consistent inflow of reactant gases across the entirety of the electrode surface. This uniform distribution cultivates balanced electrochemical reactions, maximizing the use of catalyst sites and augmenting cell performance. With both reactant gases following the same trajectory, the risk of reactant depletion close to the outlet is minimized.

On the other hand, in cell B, the counter-flow can foster the uneven distribution of reactants along electrode surfaces. Concentrations of reactants may taper off near the outlet, potentially causing localized inefficiencies and compromising overall performance. The counter-flow setup impacts mass transport dynamics. The motion of reactant gases against one another influences the rate of mass transport, potentially influencing the pace of electrochemical reactions and, consequently, the overall cell performance. Managing water becomes intricate under counter-flow conditions, as water vapor movement from cathode to anode occurs against the flow direction. This can lead to water accumulation at the cathode, affecting proton conductivity and potentially causing flooding, as shown in Figure 5. The distribution of the liquid water saturation in cell B is major through the active area of the electrode-membrane assembly.

Figure 5 Saturation distribution at the interface CL-membrane at the cathode side at 0.52 V

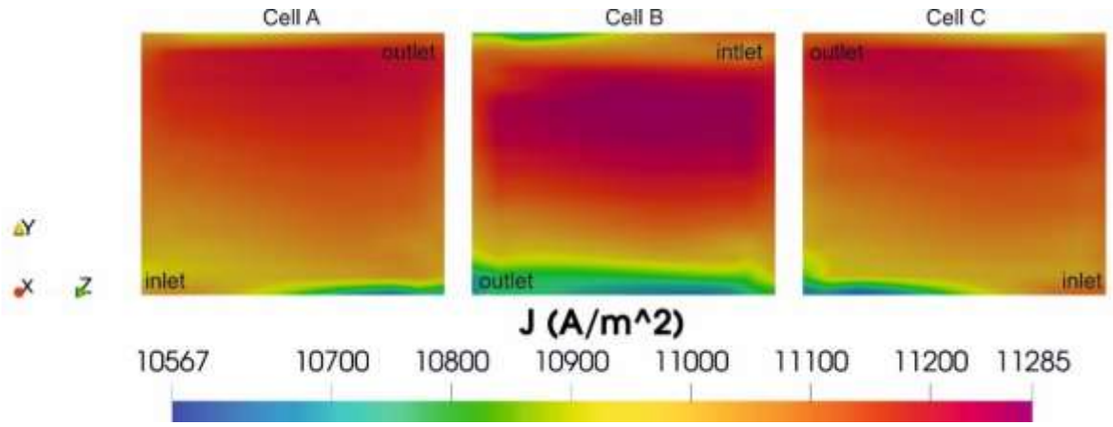

Figure 4 Current density at the interface CL-membrane at the cathode side at 0.52 V.

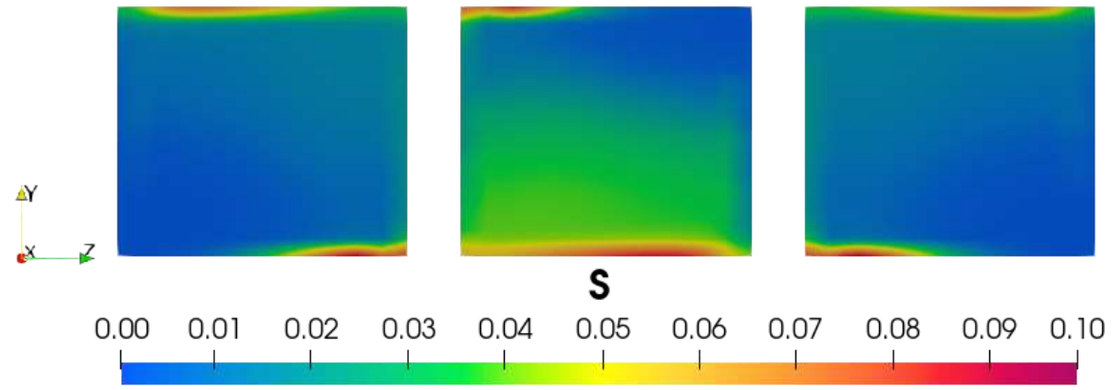

Figure 6 shows the temperature distribution where cell B exhibits an uneven temperature distribution adverse to the performance of the fuel cell. The electrochemical reactions might be more pronounced in the areas with higher temperatures, leading to accelerated degradation of the membrane and catalysts. This could result in increased resistive losses and lowered overall efficiency. The uneven temperature distribution might also indicate a cooling or thermal management issue within the fuel cell system. Addressing this abnormality is crucial to avoid long-term damage and maximize the cell's performance.

Figure 6 Temperature distribution at the interface CL-membrane at the cathode side at 0.52 V.

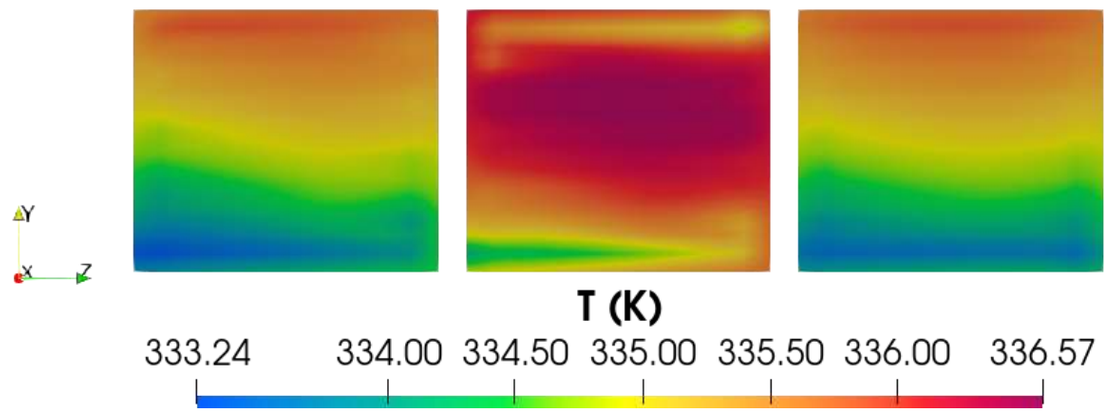

Figure 7 displays the distribution of the ionic conductivity where cell B experience a lower distribution at the zone where the cathode outlet meets the inlet of the anode side and consists of the uneven distribution of the current density and temperature in Figure 1 and 2, respectively. The electrochemical reactions within the cell are well-balanced, and the membrane conductivity is optimal. The overall efficiency is commendable, with minimal voltage losses due to resistive, activation, and mass transport losses. The temperature distribution across the cell is uniform, indicating effective cooling mechanisms and thermal management.

Figure 7 Ionic conductivity distribution at the interface CL-membrane at the cathode side at 0.52 V

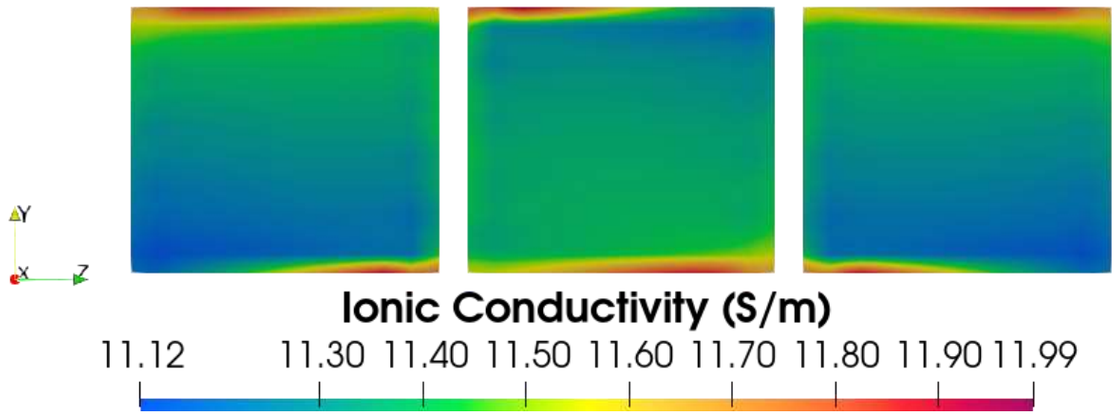

Acknowledgments

Thanks to project CONAHCYT-SENER [grant number 254667] and CONAHCYT-PhD scholarship [grant number 789267].

Conclusions

The interaction of co-flow and counter-flow configurations within serpentine channels significantly influences the performance of PEM fuel cells. Co-flow optimizes reactant distribution, staving off reactant depletion and encouraging even reactions. Meanwhile, counter-flow introduces the complexities of reactant distribution, mass transport, and water management. The selection of the most suitable flow configuration hinges on the specific requirements of the fuel cell, operational conditions, and the need to harmonize diverse performance aspects.

References

[1] Abdelkareem, M. A., Elsaid, K., Wilberforce, T., Kamil, M., Sayed, E. T., & Olabi, A. (2021). Environmentalaspects of fuel cells: A review. *Science of the Total Environment*, *752*, 141803. https://doi.org/10.1016/j.scitotenv.2020.141803

[2] Kone, J.-P., Zhang, X., Yan, Y., & Adegbite, S. (2018). An Open-Source Toolbox for Multiphase Flow Simulation in a PEM Fuel Cell. *Computer and Information Science*, *11*(3), 10. https://doi.org/10.5539/cis.v11n3p10

[3] Martins Belchor, P., Camargo Forte, M. M., & Ortiz Suman Carpenter, D. E. (2012). Parallel serpentine-baffle flow field design for water management in a proton exchange membrane fuel cell. *International Journal of Hydrogen Energy*, *37*(16), 11904–11911. https://doi.org/10.1016/j.ijhydene.2012.05.091

[4] Wang, X. D., Duan, Y. Y., Yan, W. M., & Peng, X. F. (2008). Effects of flow channel geometry on cell performance for PEM fuel cells with parallel and interdigitated flow fields. *Electrochimica Acta*, *53*(16), 5334–5343. https://doi.org/10.1016/j.electacta.2008.02.095

[5] Wang, X. D., Huang, Y. X., Cheng, C. H., Jang, J. Y., Lee, D. J., Yan, W. M., & Su, A. (2010). An inverse geometry design problem for optimization of single serpentine flow field of PEM fuel cell. *International Journal of Hydrogen Energy*, *35*(9), 4247–4257. https://doi.org/10.1016/j.ijhydene.2010.02.059